materials
SUBMITTED VERSION

Article

Collagen Coatings on Titanium: Comparative Study of Electrochemical and Chemical Formation

Marin Hodalj[1], Ines Despotović[2,*], Antonio Zandona[3], Maja Katalinić[3], Maja Ivanić[4], Jozefina Katić[1] and Željka Petrović[5,*]

[1] Department of Electrochemistry, University of Zagreb Faculty of Chemical Engineering and Technology, Zagreb, Croatia; hodaljmarin@gmail.com; jkatic@fkit.unizg.hr
[2] Division of Physical Chemistry, Ruđer Bošković Institute, Zagreb, Croatia; Ines.Despotovic@irb.hr
[3] Division of Toxicology, Institute for Medical Research and Occupational Health, Zagreb, Croatia; azandona@imi.hr; mkatalinic@imi.hr
[4] Division for Marine and Environmental Research, Ruđer Bošković Institute, Zagreb, Croatia; Maja.Ivanic@irb.hr
[5] Division of Materials Chemistry, Ruđer Bošković Institute, Zagreb, Croatia; Zeljka.Petrovic@irb.hr
* Correspondence: Ines.Despotovic@irb.hr (I.D.); Zeljka.Petrovic@irb.hr (Ž.P.)

Abstract

This study investigates the influence of two collagen-coating formation approaches, self-assembly and electrochemical formation by cyclic voltammetry, on the surface properties and electrochemical behavior of titanium (Ti). Collagen-modified Ti surfaces were characterized before and after 7 days of immersion in Fusayama artificial saliva using attenuated total reflectance Fourier-transform infrared spectroscopy, field-emission scanning electron microscopy coupled with energy-dispersive X-ray spectroscopy, X-ray diffraction, and electrochemical impedance spectroscopy. Self-assembly produced a continuous collagen layer, whereas cyclic voltammetry generated a fibrillar coating. During immersion, calcium-deficient hydroxyapatite (HAp) formed on both collagen-modified surfaces, but with distinctly different spatial organization. The self-assembled coating underwent reorganization, whereas the electrochemically formed coating retained its fibrillar framework closely associated with the HAp phase. This organic–inorganic architecture was accompanied by enhanced barrier properties after 7 days compared with the self-assembled coating. Density functional theory calculations further showed that one-electron oxidation of an adsorbed collagen-model tripeptide induces pronounced structural rearrangement, providing molecular-level insight into the redox response of collagen-derived species at the TiO_2 interface. In addition, prolonged exposure of Ti surfaces to cell culture media resulted in negligible Ti release, while the resulting conditioned media showed no significant impairment of HGF-1 or MG-63 cell viability, supporting favorable indirect in vitro cytocompatibility under the investigated conditions.

Keywords: titanium; collagen; cyclic voltammetry; self-assembly; DFT; cytocompatibility

Academic Editor: Firstname Lastname

Received: date
Revised: date
Accepted: date
Published: date

Copyright: © 2026 by the authors. Submitted for possible open access publication under the terms and conditions of the Creative Commons Attribution (CC BY) license.

1. Introduction

The surface properties of implant materials play a critical role in the initial interactions with the surrounding biological environment. For titanium (Ti), widely used in dental implantology, physicochemical surface characteristics strongly influence cell–material interactions and subsequent tissue responses. Early studies demonstrated that Ti surface

roughness can alter the response of osteoblast-like cells [1] and influence bone–implant contact in vivo [2]. These findings have motivated the development of various surface modification and functionalization strategies aimed at tailoring the implant–tissue interface and enhancing its biological performance [3].

Surface modification techniques are broadly categorized into physical, chemical, and biological approaches, each providing different means of tailoring the implant surface and its interaction with the surrounding tissue [3,4]. Physical and chemical treatments, such as sandblasting, acid etching, and micro-arc oxidation, are used to modify the surface topography, morphology, and physicochemical properties of Ti [5,6]. In addition to these treatments, functional coatings provide an alternative approach to tailoring the implant–tissue interface by introducing bioactive components that can influence cellular responses [4]. Such coatings include inorganic materials, particularly calcium phosphates [7], as well as bioactive organic components, including growth factors such as bone morphogenetic proteins [8] and extracellular matrix (ECM) proteins such as collagen [9].

Among biomolecules used for surface functionalization, collagen, a major structural component of the extracellular matrix, is of particular interest for the biofunctionalization of Ti surfaces. Collagen-based coatings have shown potential to promote osseointegration [10]. In vivo studies have shown that type I collagen-functionalized Ti surfaces can enhance early bone formation and osteogenic differentiation [11], improve osseointegration [12], and promote bone maturation and mineralization at the implant–bone interface [13].

The method used to form collagen coatings on Ti surfaces can influence coating´s stability and interfacial properties [14]. Different strategies have been developed, including physical adsorption, self-assembly, covalent immobilization, and electrically assisted approaches [14–17]. Physical adsorption represents a relatively simple approach, whereas covalent immobilization generally requires prior surface activation and chemical functionalization. Marín-Pareja et al. compared physical adsorption of type I collagen on activated Ti surfaces with covalent immobilization through organosilane chemistry and showed that the amount and stability of immobilized collagen depended on both the immobilization method and the surface activation treatment [14]. Gregurec et al. prepared collagen–alginate films on titania by layer-by-layer self-assembly followed by chemical crosslinking, resulting in stable coatings with a fibrillar morphology [15]. In our previous study, hydrolyzed collagen alone was self-assembled on Ti from an aqueous solution followed by post-thermal treatment, and the resulting coating exhibited high electrochemical barrier properties in artificial saliva [16].

Electrically assisted deposition has also been explored for collagen coating formation on Ti. Wang et al. employed electrophoretic deposition (EPD) to form a type I collagen coating on Ti, which was subsequently subjected to biomimetic mineralization [17]. Potential-controlled electrodeposition has also been employed for collagen immobilization on Ti. Kamata et al. investigated collagen electrodeposition under different pH, potential, and deposition-time conditions and found that alternating-potential deposition between −1 and +1 V vs the saturated calomel electrode (SCE) produced a durable and relatively uniform collagen layer compared with conventional immersion [18]. More recently, electrochemical deposition of collagen fibrils on Ti was shown to provide high electrochemical barrier properties and to promote calcium phosphate nucleation in artificial saliva [19].

Although electrochemical methods have been used for collagen coating formation, cyclic voltammetry, to the best of our knowledge, has not previously been explored for this purpose on Ti surfaces. At the same time, molecular-level understanding of electrochemically assisted collagen coating formation remains limited, despite recent efforts to correlate experimental observations with theoretical calculations [19]. Moreover, although immersion-based and electrochemically assisted approaches to collagen immobilization have been reported, a direct comparison of collagen coatings formed by self-assembly and

cyclic voltammetry, including their structural differences, mineralization and electrochemical behavior in artificial saliva, is still lacking.

Therefore, this study compares collagen coatings formed on Ti by self-assembly and cyclic voltammetry, examining how the formation route influences coating architecture and how the resulting coatings subsequently evolve during exposure to artificial saliva. Surface, structural, and electrochemical characterization was complemented by density functional theory (DFT) calculations examining the redox behavior and oxidation-induced structural changes of an adsorbed collagen-model tripeptide at the TiO_2 interface. Ti release during prolonged exposure to cell culture media and indirect cytocompatibility were additionally evaluated on human gingival fibroblasts and osteoblast-like cells to provide an initial assessment of the biological response under the investigated conditions.

2. Materials and Methods

2.1. Materials, chemicals and solutions

Titanium (Ti) rod, cut into discs (⌀ = 12 mm; 99.9%; Alfa Aesar®, Karlsruhe, Germany), served as substrates for the collagen coating. Before coating formation, the Ti surface was mechanically abraded with SiC emery papers of grit sizes #180, #240, #500, and #600, ultrasonically cleaned for 5 min with absolute ethanol (p.a.; Gram-Mol®, Zagreb, Croatia), acetone (p.a.; Gram-Mol®, Zagreb, Croatia), and MilliQ water (Hydrolab, Wesoła, Straszyn, Poland, 0.05 ⌾S/cm). The Ti substrates were then dried in a nitrogen stream (99.999%, Messer, Germany) and exposed to air for 10 min before coating formation.

An aqueous solution of animal-derived hydrolyzed collagen (HC; approximately 45 mg mL^{-1}, corresponding to a nominal concentration of 10^{-2} mol dm^{-3} based on an estimated average molar mass of 4.5 kDa; Medex d.o.o., Ljubljana, Slovenia) was used for coating´s preparation. The pH of the solution was 4.4.

Fusayama artificial saliva was prepared from the following chemicals without further purification: NaCl (p.a.; Kemika®, Zagreb, Croatia), KCl (p.a.; Kemika®, Zagreb, Croatia), $CaCl_2 \cdot 2H_2O$ (p.a.; Kemika®, Zagreb, Croatia), $Na_2HPO_4 \cdot 2H_2O$ (p.a.; Kemika®, Zagreb, Croatia), and urea (p.a.; Kemika®, Zagreb, Croatia). The pH was 6.8 [20].

2.2. The preparation of collagen coatings on Ti substrates

The collagen coating was formed in two ways: (i) chemically by self-assembly and (ii) electrochemically by cyclic voltammetry at 25 ± 3 °C.

Chemical formation by self-assembly. For the coating prepared by self-assembly, the Ti discs were immersed in the hydrolyzed collagen solution for 24 hours. The Ti samples modified by self-assembly are labeled Ti/collagen SAM.

Electrochemical formation by cyclic voltammetry. The electrochemical formation of the collagen coating was carried out in a three-electrode cell, with the Ti sample (an exposed area of 1 cm^2) as the working electrode, Ag/AgCl/3 M KCl as the reference electrode with a potential of 0.210 V versus the standard hydrogen electrode, and a graphite rod as the counter electrode. The potential range for coating formation was selected based on the cyclic voltammogram of Ti recorded in the HC solution. The initial cyclic voltammogram was recorded over the potential range from −0.3 to 0.5 V at 50 mV s^{-1}, and the potential range from −0.3 to 0.1 V was selected for coating formation. The collagen coating was formed by cycling the Ti electrode between −0.3 and 0.1 V, starting and ending at the open circuit potential (OCP), at a scan rate of 10 mV s^{-1} for 20 cycles. The measurements were performed using an Autolab 128 N potentiostat/galvanostat (Metrohm Autolab B.V., Utrecht, The Netherlands) controlled by Nova® 2.1.8 software (Metrohm Autolab B.V.,

Utrecht, The Netherlands). The samples are labeled Ti/collagen CV. After coating formation, the samples were briefly rinsed by immersion in water and then allowed to dry in air.

2.3. Characterization of the unmodified and collagen-modified Ti substrates

The morphological characteristics of unmodified and modified Ti substrates were investigated using field emission scanning electron microscopy (FE-SEM, model JSM-7000F, JEOL Ltd., Tokyo, Japan) in conjunction with an EDS/INCA 350 energy dispersive X-ray analyzer (Oxford Instruments, High Wycombe, UK) to determine the elemental composition of the Ti surfaces. Since the energies of the N Kα (0.392 keV) and Ti Lα (0.452 keV) [21] lines are close to each other, an accelerating voltage of 5 kV was used to reduce the contribution of the Ti substrate and enhance the relative contribution of the near-surface collagen layer.

The chemical characteristics of the unmodified and modified Ti surfaces were monitored using attenuated total reflection Fourier transform infrared spectroscopy (ATR-FTIR). Spectra were recorded with the Frontier spectrometer (PerkinElmer, Waltham, MA, USA) from 4000 to 400 cm^{-1} at a resolution of 4 cm^{-1} and 20 scans per measurement.

The phase composition of the deposits on unmodified and modified Ti surfaces after 7 days of exposure to artificial saliva was analyzed using the Empyrean X-ray diffractometer, model 3 (XRD, Malvern Panalytical B.V., Almelo, The Netherlands), in the 2θ range between 10° and 90°, at 45 kV and 40 mA, with CuKα radiation (λ = 0.1542 nm).

The influence of collagen coating on the electrochemical behavior of Ti in Fusayama artificial saliva was investigated by electrochemical impedance spectroscopy (EIS) at the OCP. Before EIS measurements, the samples were allowed to stabilize at OCP for 1 h. The measurements were performed in the same three-electrode cell configuration used for electrochemical coating formation, with the Ti sample (an exposed area of 1 cm^2) as the working electrode, Ag/AgCl/3 M KCl as the reference electrode, and a graphite rod as the counter electrode. EIS spectra were recorded in the frequency range from 10^5 to 10^{-3} Hz using an AC amplitude of 10 mV with a PalmSens4 potentiostat/galvanostat/frequency analyzer and PSTrace 5.13 software (PalmSens BV, Netherlands). The EIS data were fitted using the same software.

2.4. The Quantum-chemical DFT calculations

To model a hydrolyzed collagen molecule, a functional tripeptide fragment, Gly–Pro–Hyp was used, following our previously established computational approach [19]. Based on the charge characteristics of hydrolyzed collagen at the experimental solution pH and its previously observed anodic deposition behavior [19], the tripeptide was modelled in its anionic form, NH_2–Gly–Pro–Hyp–COO^-. As in our previous computational study [19], a $(TiO_2)_{10}$ nanocluster, originally employed by Qu and Kroes [22], was used to model the native titanium oxide surface.

The molecular-level insight into the electrochemical oxidation of the collagen-derived tripeptide on the titanium surface, its redox properties and structural changes upon oxidation was obtained by utilizing the quantum chemical DFT calculations [23,24]. The relevant TiO_2/tripeptide configurations were optimized by employing the M06 functional developed by Truhlar's group [25-27] with 6-31+G(d,p) + LANL2DZ basis set. Pople's 6-31+G(d,p) double-ξ basis set was chosen for the H, C, O and N atoms, and the LANL2DZ basis set was chosen for the transition metal (Ti) atoms [28]. The configuration of the TiO_2 cluster was kept fixed during the geometry optimizations of both the anionic and radical species. All the calculated structures were verified to be true minima on the potential en-

ergy surface via vibrational frequency analysis under the harmonic oscillator approximation, and the thermal correction to the Gibbs free energy was derived from the same vibrational analysis. The final energy calculations were performed by utilizing a highly flexible 6-311++G(2df,2pd) basis set for the H, C, O and N atoms, whereas the same LANL2DZ ECP type basis set was used for the titanium atoms. The solvation effects were taken into account by employing the polarizable continuum solvation model SMD (Solvation model based on density) [29]. The water solvent is represented by a dielectric constant of ε = 78.3553. All calculations were carried out using the program package Gaussian 16 (revision C.01) [30].

The topological analysis of the charge density distribution was accomplished by means of Bader's quantum theory of atoms in molecules (QTAIM) [31] using the program package AIMALL [32] and the SMD/M06/6-31+G(d,p) + LANL2DZ wave function obtained from the optimization.

The reaction Gibbs free energy, $\Delta_r G^*$, was calculated via the equation $\Delta_r G^* = G^*_{AB} - G^*_A - G^*_B$, where G^*_{AB} is the total free energy of the resulting AB structure and G^*_A and G^*_B are the total free energies of the interacting units A and B, respectively.

The equilibrium redox potential was calculated according to equation: $E = -\Delta_r G^*/nF$ where $\Delta_r G^*$ is the Gibbs free-energy change, n is the number of transferred electrons, and F is the Faraday constant (96.485 C/mol). Following the reduction convention for reporting electrode potentials [33] the $(TiO_2)_{10}$—tripeptide•/$(TiO_2)_{10}$—tripeptide$^-$ redox couple was represented by the reduction half-reaction defined as: $(TiO_2)_{10}$—tripeptide• + e^- → $(TiO_2)_{10}$—tripeptide$^-$. The calculated potential was referenced to the Ag/AgCl/3 M KCl reference electrode using the absolute potential of the standard hydrogen electrode (4.44 V) [34] and the standard potential of the Ag/AgCl/3 M KCl electrode +0.210 V vs. SHE [35].

2.5. Chemical stability and cytocompatibility assessment

Based on a literature report in which collagen-coated Ti surfaces were subjected to gamma irradiation at 12 kGy before in vitro experiments [36], the effect of gamma irradiation on the collagen SAM and CV coatings was evaluated at doses of 8, 10, and 15 kGy using a Cobalt-60 gamma source located at the Radiation Chemistry and Dosimetry Laboratory of the Ruđer Bošković Institute. The surface morphology was examined by SEM before and after irradiation, and no evident morphological changes in the coatings were observed at any of the investigated doses. Therefore, the highest tested dose, 15 kGy, was selected for sterilization of the samples used in the subsequent cell-based experiments.

The samples were then incubated in two cell culture media (Dulbecco's Modified Eagle's Medium (DMEM) and Eagle's Minimum Essential Medium (EMEM), Sigma-Aldrich, Steinheim, Germany) either supplemented with fetal bovine serum (FBS, Sigma-Aldrich, Steinheim, Germany) or under serum-free conditions for 90 days. Aliquots of the conditioned media were collected after 1, 7, 14, 28, 60, and 90 days of incubation and subsequently analyzed by inductively coupled plasma mass spectrometry (8900 ICP-QQQ, Agilent, USA) to assess Ti release into the culture medium and for the assessment of cell viability. For ICP-QQQ analysis, samples were acidified with HNO_3 (65%, Suprapur, Merck, Darmstadt, Germany) and left overnight before being diluted to a final volume of 10 mL with Milli-Q water. Indium (50 $\mu g\ L^{-1}$) was used as an internal standard.

Human gingival fibroblasts (HGF-1, CRL-2014™, ATCC, Manassas, VA, USA) and human osteoblast-like cells (MG-63, CRL-1427™, ATCC, Manassas, VA, USA) were cultured in Dulbecco's Modified Eagle's Medium (DMEM) or Eagle's Minimum Essential Medium (EMEM) supplemented with 10% (v/v) fetal bovine serum (FBS), and 1% (v/v) penicillin/streptomycin (PenStrep solution), respectively. The mentioned culture reagents

were obtained from Sigma-Aldrich, Steinheim, Germany. Cell cultures were grown at 37 °C in a 5% CO_2 atmosphere. The growth medium was replaced every two days. The passage of cells was performed in line with the manufacturer's recommendations. Cells were detached with 0.25% trypsin/EDTA solution (Sigma-Aldrich, Steinheim, Germany), resuspended, and seeded 24 h before experiments. The viability assay (CellTiter-Glo® Luminescent Cell Viability Assay, Promega, Madison, WI, USA) followed the procedure presented previously [37]. Briefly, 10,000 cells per well were seeded in 96-well opaque plates and exposed for 24 h to conditioned media, either serum-free or FBS-supplemented, collected at defined time points of incubation period from unmodified and collagen-modified titanium samples as described in the previous paragraph. After 24 h exposure of cells, the reagent was added, and luminescence was recorded using a microplate reader (SpectraMax® iD3, Molecular Devices, San Jose, CA, USA). Data were taken from at least two experiments and plotted as a percentage of viable cells relative to untreated control cells.

2.6. Use of Generative Artificial Intelligence

During the preparation of this manuscript, the authors used OpenAI ChatGPT (GPT-5.6 Sol) for the visual composition and design of the Graphical Abstract based on the original concept and scientific content provided by the authors. All experimental data presented in the Graphical Abstract, including SEM micrographs and electrochemical impedance spectroscopy results, were generated by the authors and incorporated without alteration. The authors reviewed and edited the output and take full responsibility for the content of this publication.

3. Results and discussion

3.1. Electrochemical formation of the collagen coating (Ti/collagen CV)

The potential range for collagen CV coating formation was selected based on a cyclic voltammogram of Ti recorded in the HC solution over a wider potential window (−0.3 to +0.5 V) at a scan rate of 50 mV s^{-1} (Figure 1a). Within this voltammogram, the potential range from −0.3 to +0.1 V was characterized by relatively low current densities and the absence of the pronounced anodic current increase observed at more positive potentials. This range was therefore selected for subsequent collagen coating formation by cyclic voltammetry, using 20 cycles at a scan rate of 10 mV s^{-1} (Figure 1b).

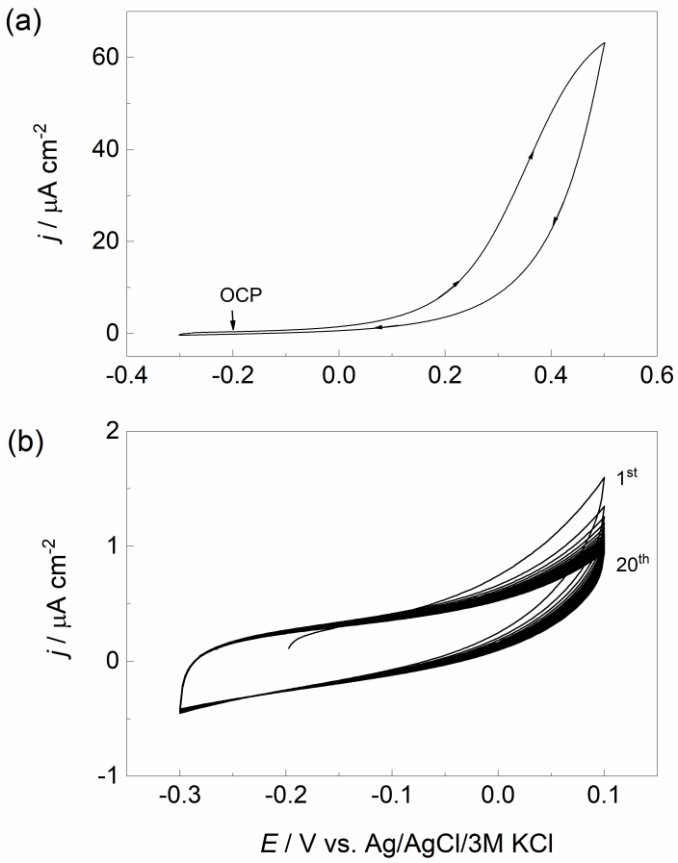


Figure 1. Cyclic voltammetric responses of Ti in the HC solution: (a) cyclic voltammogram recorded over a wider potential range at a scan rate of 50 mV s^{-1}; (b) evolution of the cyclic voltammetric response during 20 cycles within the selected coating-formation potential range at a scan rate of 10 mV s^{-1}.

3.2. Molecular-level insight into the redox behavior and structural response of the adsorbed collagen model

To gain molecular-level insight into the redox behavior and oxidation-induced structural changes of hydrolyzed collagen-derived species adsorbed on the TiO_2 surface, DFT calculations were performed. The electrochemical oxidation of the modelled anionic tripeptide (NH_2-Gly-Pro-Hyp-COO^-) adsorbed on a TiO_2 cluster may represent not only an electron-transfer process but also a chemical activation step facilitating intermolecular coupling. After conversion to the Ag/AgCl/3M KCl reference scale, the corresponding calculated oxidation potential was +0.458 V. This potential lies within the more positive region of the wide-range cyclic voltammogram in which a pronounced increase in anodic current was observed (Figure 1a). However, this current increase cannot be assigned specifically to collagen oxidation because electrochemical processes associated with the Ti/TiO_2 surface may also contribute to the anodic response. Moreover, the calculated oxidation potential is more positive than the upper vertex potential (+0.1 V) used for collagen coating formation in the present study. Therefore, the calculated oxidation process should not be regarded as direct evidence for the mechanism of collagen coating formation under the applied CV conditions. Upon one-electron oxidation, the anionic tripeptide formally gives rise to a neutral radical species that exhibits pronounced changes in molecular geometry.

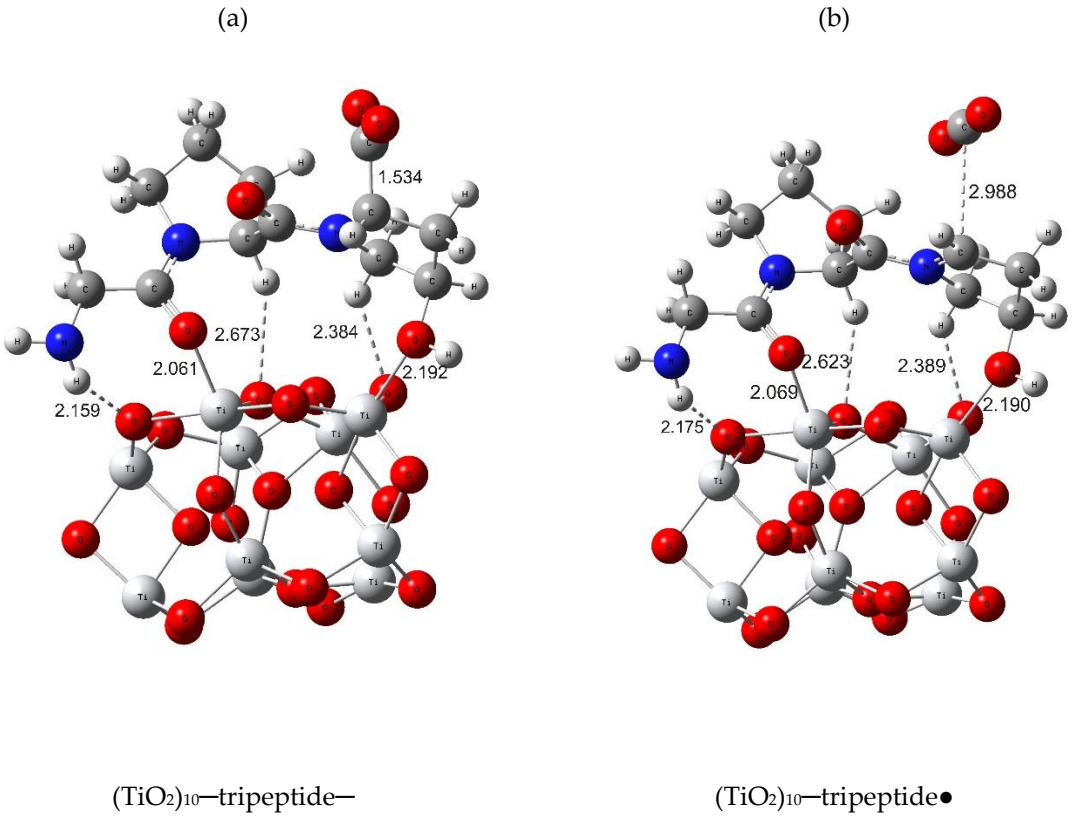


Figure 2. Optimized structures of the (a) anionic tripeptide adsorbed on the $(TiO_2)_{10}$ cluster, $(TiO_2)_{10}$—tripeptide^{-}, and the (b) corresponding neutral radical, $(TiO_2)_{10}$—tripeptide$^{\bullet}$, formed upon one-electron oxidation. Selected bond lengths are indicated in Å. Color code: Ti - light gray; O – red; C – gray; N – blue; H – white.

A particularly relevant structural change is the substantial elongation of the C–C bond linking the hydroxyproline ring to its carboxylate carbon, from 1.534 Å in the anionic state to 2.988 Å in the radical state (Figure 2). This elongation, accompanied by a rearrangement of the COO^{-} group, i.e. its substantial linearization, may increase the accessibility of the carboxylate moiety and facilitate its interaction with the nucleophilic nitrogen atom of the terminal amino group of a neighboring tripeptide. Importantly, AIM analysis indicates that the C–C interaction persists in the radical state, suggesting substantial bond elongation rather than complete dissociation of the carboxylate-containing moiety. The calculated oxidation-induced structural rearrangement may create a more favorable geometry for intermolecular C–N bond formation. Since the carboxylate group remains within the molecular structure, such a rearrangement could facilitate intermolecular coupling and the formation of longer peptide-like chains. However, such coupling should therefore be regarded as a possible consequence of the predicted structural rearrangement rather than an established reaction pathway.

This hypothesis may help explain the distinct coating morphologies obtained by electrochemical deposition and self-assembly (Section 3.3). Whereas self-assembly primarily promotes molecular organization at the surface, electrochemical polarization may additionally induce electronic and structural changes in the adsorbed tripeptide that favor intermolecular coupling. The TiO_2 surface may further contribute by providing a template for molecular orientation and accumulation. The calculated oxidation potential (+0.458 V vs Ag/AgCl/3 M KCl) lies above the upper vertex potential (+0.1 V) applied during CV coating formation, therefore the present calculations provide molecular-level insight into the oxidation-induced structural response of the adsorbed tripeptide but do not establish

this oxidation pathway as the mechanism responsible for the fibrillar coating morphology observed experimentally.

Overall, the DFT results suggest that electrochemical oxidation can induce substantial structural reorganization of the adsorbed tripeptide, potentially facilitating intermolecular coupling and subsequent chain growth. These molecular changes may contribute to the formation of different coating´s morphologies observed experimentally for Ti/collagen CV compared with Ti/collagen SAM.

3.3. Chemical characterization and morphology of Ti/collagen SAM and Ti/collagen CV coatings

ATR-FTIR analysis. To verify the presence of collagen on the Ti surface, the surfaces were analyzed by ATR-FTIR spectroscopy, and the results are shown in Figure 3. In addition to the modified Ti surfaces, Ti/collagen SAM and Ti/collagen CV, a bare Ti surface was also analyzed as a reference sample. Compared with bare Ti, both collagen-modified surfaces show a complex, very similar response, with characteristic absorption bands assigned to the collagen structure. The observed bands correspond to the characteristic amide bands A_A, A_I, A_{II}, A_{III}, A_{IV}, and A_V, as previously described [19,38,39].

Briefly, the amide A_A, A_I, A_{II}, A_{III}, A_{IV}, and A_V bands were observed at approximately 3298, 1646, 1549, 1240, 551, and 622 cm^{-1}, respectively. The A_I band position corresponds well to that observed for the hydrolyzed collagen powder used for coating preparation [19]. The bands marked with * in the 1400–1200 cm^{-1} region can be assigned to CH_2 wagging vibrations of glycine and proline [19]. The presence of these characteristic bands on both Ti/collagen SAM and Ti/collagen CV surfaces confirms the presence of collagen on the Ti surface by both preparation methods.

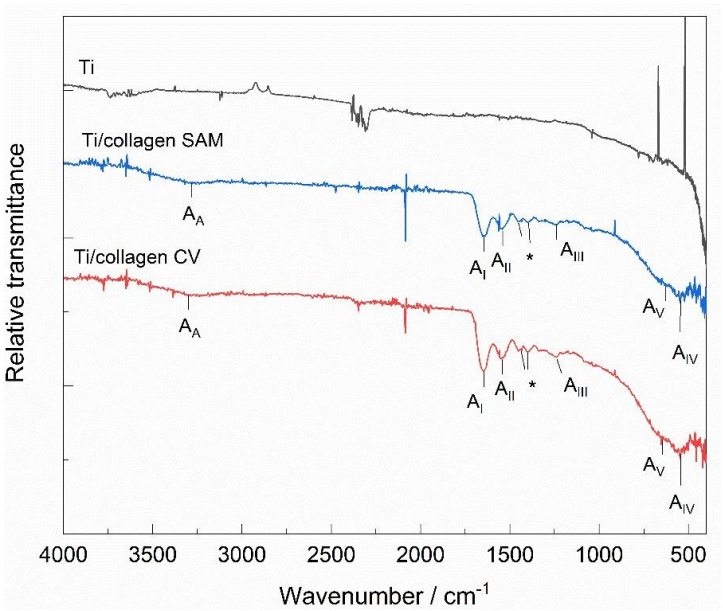


Figure 3. ATR-FTIR spectra of bare Ti and Ti modified with collagen prepared by self-assembly (Ti/collagen SAM) and cyclic voltammetry (Ti/collagen CV).

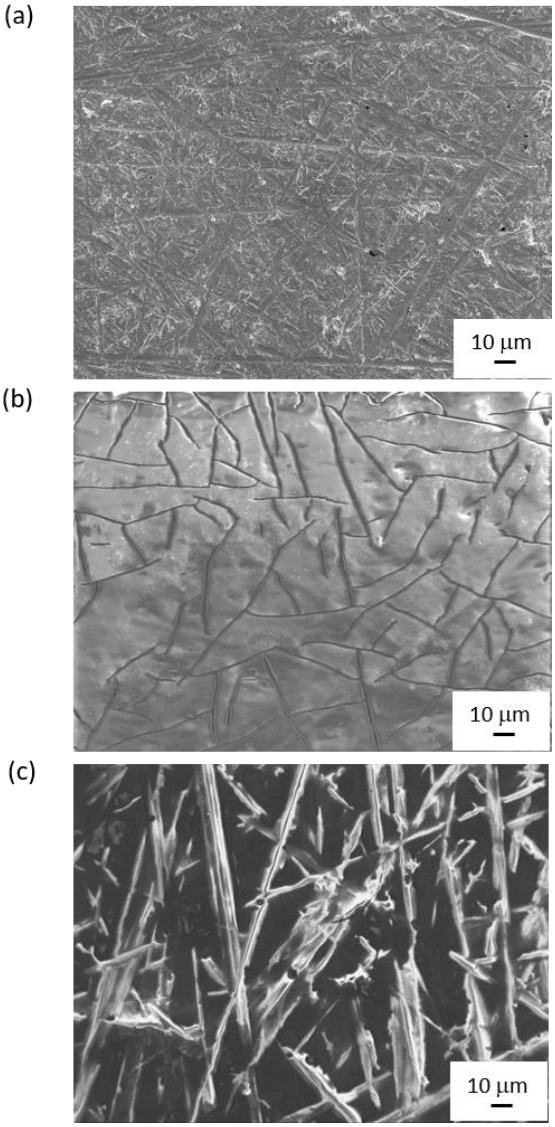
FE-SEM analysis. Having confirmed the presence of collagen coatings on the Ti surface, the influence of the formation method on the morphology of the resulting coatings was subsequently investigated by FE-SEM. Figs. 4a-c show the morphology of the unmodified Ti surface as well as surfaces modified with collagen coatings, Ti/collagen SAM and Ti/collagen CV.

The images clearly show that the collagen coating, regardless of the formation method, alters the morphology of the Ti surface characterized by marks resulting from

mechanical surface treatment (Fig. 4a). Self-assembly produces a continuous layer with large island-like structures and pronounced cracks (Fig. 4b). The formation of a continuous layer may be attributed to the prolonged exposure of the Ti surface to the HC solution for 24 h, which enables gradual adsorption and organization of collagen molecules on the surface. The cracks observed in the SAM coating may be associated with drying-induced contraction of the collagen layer after removal from the solution.

In contrast to the SAM coating, the electrochemical method produces a distinctly different morphology dominated by a fibrous collagen structure, with visible fiber overlapping and the formation of a network-like structure (Fig. 4c). The fibers are elongated and, in some areas, appear to coalesce into thicker structures. The resulting morphology may be related to the applied potential and repetitive cycling, which may affect not only the transport of collagen molecules to the surface and their organization into a fibrous structure but also the subsequent association and reorganization of the fibers into network-like and thicker structures [40].

Recent studies have shown that fibrous collagen architecture on metallic substrates is difficult to achieve without cross-linking agents or additional chemical or processing steps [41,42]. Therefore, the results obtained are of particular significance, as a fibrous collagen coating was formed by a relatively simple electrochemical process from an aqueous solution of hydrolyzed collagen, without the use of additional chemicals or complex processing steps.



.

Figure 4. FE-SEM images of (a) the bare Ti surface and Ti surfaces modified with collagen prepared by (b) self-assembly (Ti/collagen SAM) and (c) cyclic voltammetry (Ti/collagen CV). The micrographs were recorded at an accelerating voltage of 5 kV and a magnification of 500×.

EDS analysis. Complementary evidence for the presence of collagen was obtained by EDS analysis, and the results are shown in Figure 5. The EDS spectrum of bare Ti was dominated by the Ti signal, as expected. For the collagen-modified surfaces, measurements were performed at 5 kV specifically to enhance surface sensitivity. Both Ti/collagen SAM and Ti/collagen CV showed detectable carbon, nitrogen, and oxygen signals, consistent with the presence of the collagen coating.

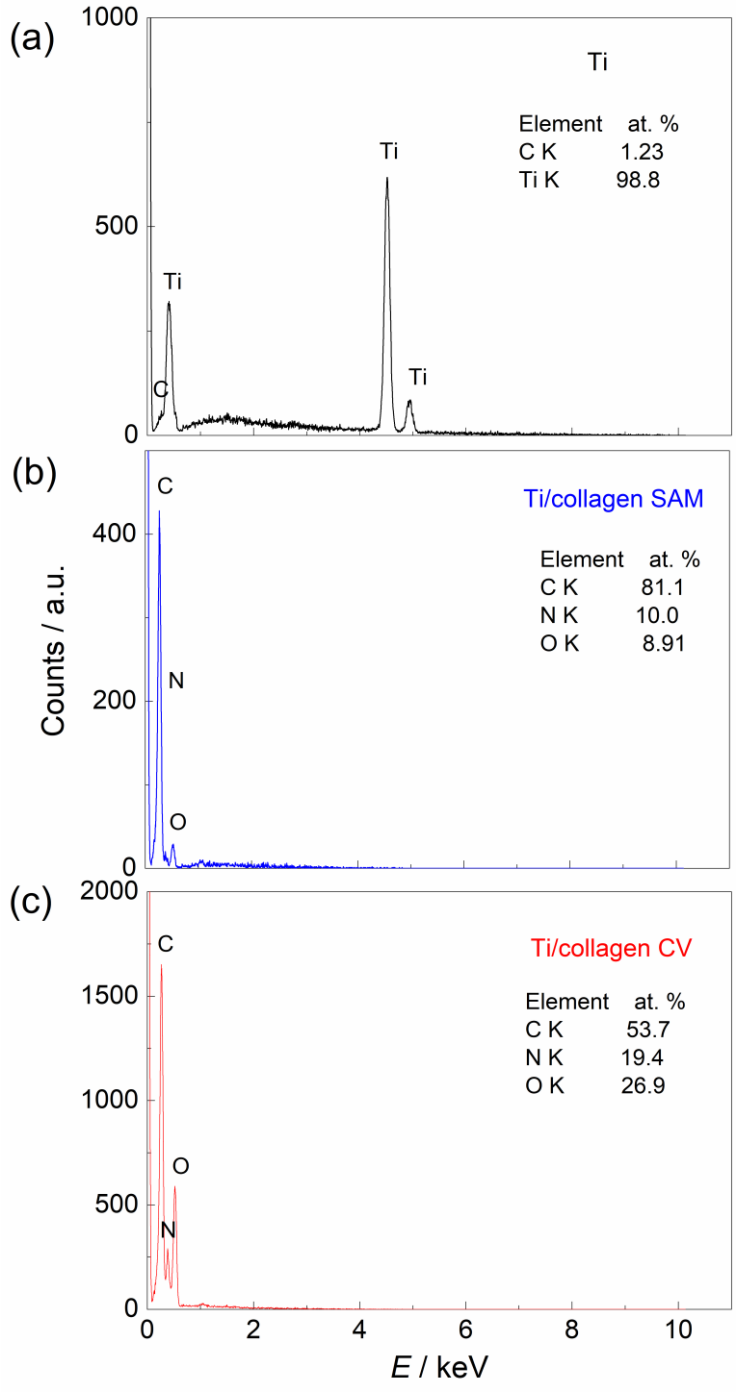


Figure 5. EDS spectra of (a) bare Ti, (b) (Ti/collagen SAM), and (c) (Ti/collagen CV) surfaces.

3.4. Characterization of collagen-modified Ti samples after immersion in Fusayama artificial saliva

To investigate the behavior of collagen-modified Ti samples in a simulated physiological environment, the samples were immersed in Fusayama artificial saliva at room temperature for 7 days. After this period, the samples were removed, air-dried, and subjected to chemical, morphological, phase, and electrochemical characterization using ATR-FTIR, EDS, FE-SEM, XRD, and EIS. To determine the influence of the collagen coating, the same characterization was performed under identical conditions on bare Ti.

ATR-FTIR analysis. The results of the chemical characterization performed by ATR-FTIR are shown in Figure 6.

As shown in Figure 6, after 7 days of immersion in Fusayama artificial saliva, collagen-related bands remained detectable on both modified surfaces. In particular, the characteristic A_I band at approximately 1630 cm^{-1} and the band associated with CH_2 vibrations of glycine and proline, marked with *, at approximately 1460 cm^{-1} were observed (see Figure 3). At the same time, new bands appeared in the spectra of all three samples, indicating the formation of new surface species during immersion. The observed bands can be associated with calcium phosphate (CaP) phases, consistent with the formation of CaP-containing surface deposits on all investigated Ti surfaces [43]. In addition, the broad band at approximately 3353 cm^{-1} for the Ti/collagen CV and 3372 cm^{-1} for the Ti/collagen SAM can be associated with O–H stretching vibrations of hydrogen-bonded water, while the band around 1660 cm^{-1} can be attributed to the bending vibration of adsorbed water molecules [39].

The ATR-FTIR results indicate that the collagen material remained present after 7 days of immersion, regardless of the formation method, and simultaneously indicate the formation of a CaP layer on both unmodified and collagen-modified Ti. Notably, the CaP-related bands are more pronounced for the collagen-modified surfaces than for bare Ti, suggesting that collagen may favor CaP formation under the investigated immersion conditions.

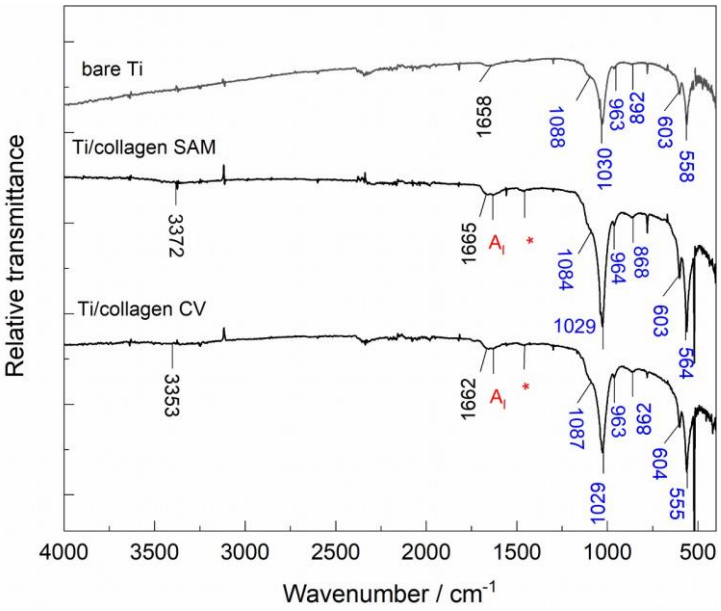


Figure 6. ATR-FTIR spectra of bare Ti and Ti modified with collagen prepared by self-assembly (Ti/collagen SAM) and cyclic voltammetry (Ti/collagen CV), recorded after immersion in Fusayama artificial saliva. Collagen-related bands are highlighted in red, CaP-related bands in blue, and water-related bands in black.

FE-SEM analysis. The microstructural features of the CaP-containing surface layers formed on all investigated samples after 7 days of immersion in Fusayama artificial saliva were investigated by FE-SEM, and the corresponding images are shown in Figure 7.

The FE-SEM images reveal differences in the morphology and distribution of the CaP layers formed after 7 days of immersion. On bare Ti, CaP deposits appear as localized irregular structures distributed over the mechanically treated Ti surface. In contrast, the collagen-modified surfaces show more extensive coverage by CaP deposits, which is consistent with the more pronounced bands visible in the ATR-FTIR spectra (Figure 6). For Ti/collagen SAM, the initially continuous collagen layer (Figure 4b) undergoes pronounced morphological reorganization during immersion. The collagen-related material appears to accumulate locally into thicker structures (Figure 7d, inset; supported by EDS, Figure 8d), while areas of the underlying Ti surface remain exposed between these SAM- and CaP-structures. The CaP deposits are predominantly observed on the exposed Ti surface areas.

A distinct morphology is observed for Ti/collagen CV. The fibrillar collagen structure remains clearly recognizable after 7 days of immersion, while CaP-containing deposits appear to preferentially form along the fibrillar structure and partially cover the collagen fibers (Figures 7e, f). This association of the mineral deposits with the collagen fibrillar structure is consistent with the previously reported role of collagen functional groups in promoting the adsorption of calcium and phosphate species and facilitating subsequent mineral formation [19]. The rod-like/needle-like morphology of the CaP deposits can be observed on both collagen-modified surfaces, although the overall organization and distribution of the deposits differ between the Ti/collagen SAM and Ti/collagen CV surfaces. The inset in Figure 7f shows a cluster of needle-like particles forming the CaP-containing deposit. Based on the literature, this morphology can be related to hydroxyapatite formation, while hydroxyapatite with hexagonal symmetry preferentially grows along the c-axis and may exhibit plate-like or needle-like morphologies when precipitated without a template [44].

Overall, the SEM results indicate that the collagen coatings do not remain unchanged during immersion. Instead, both coatings undergo morphological reorganization accompanied by CaP formation. While the SAM coating undergoes local reorganization and partial detachment from the Ti surface during immersion, the electrochemically prepared coating partially retains its initial fibrillar morphology, which becomes embedded within the newly formed CaP layer. This behavior may be advantageous from a biomaterials perspective, as the coexistence of a retained collagen fibrillar framework and an inorganic CaP phase resembles aspects of the organic–inorganic organization characteristic of bone tissue.

EDS analysis. Detailed elemental analysis of the CaP deposits formed on bare and collagen-modified Ti surfaces was performed by EDS analysis (Figure 8).

The CaP deposits identified on all investigated surfaces contain Ca, P and O, together with Na, K and Cl in varying proportions. These results are consistent with the ATR-FTIR and FE-SEM data, supporting the presence of CaP deposits on all surfaces. In addition, nitrogen was detected on both collagen-modified surfaces, providing further evidence of detectable collagen elements after 7 days of immersion. The average Ca/P atomic ratios obtained from three measurements were 1.01 for bare Ti, 1.44 for Ti/collagen SAM and 1.39 for Ti/collagen CV. Thus, both collagen-modified surfaces exhibited higher Ca/P ratios than bare Ti, with comparable values for the two coating formation methods.

For the Ti/collagen SAM surface, two representative EDS spectra were recorded from distinct surface regions (Figure 8c,d). The spectrum obtained from the CaP-covered region (Figure 7c) shows the presence of Ca and P, whereas the spectrum recorded from the detached, collagen-rich structure shown in the SEM inset (Figure 7d) is dominated by C and

O, with a detectable N signal (~5 at.%) and no detectable Ca or P. The elemental composition of this structure further supports its assignment as a collagen-containing residue remaining on the Ti surface after immersion. Thus, the EDS results indicate that a fraction of the collagen-rich material on the SAM surface remained spatially separated from the CaP deposit.

In contrast, the fibrillar structure of the Ti/collagen CV coating remained closely associated with the CaP deposits after immersion, as observed by FE-SEM (Figures 7e,f) and supported by the corresponding EDS results (Figure 8b). Thus, the electrochemically formed coating appears to provide a closer spatial association between the retained collagen fibrillar framework and the newly formed inorganic CaP phase.

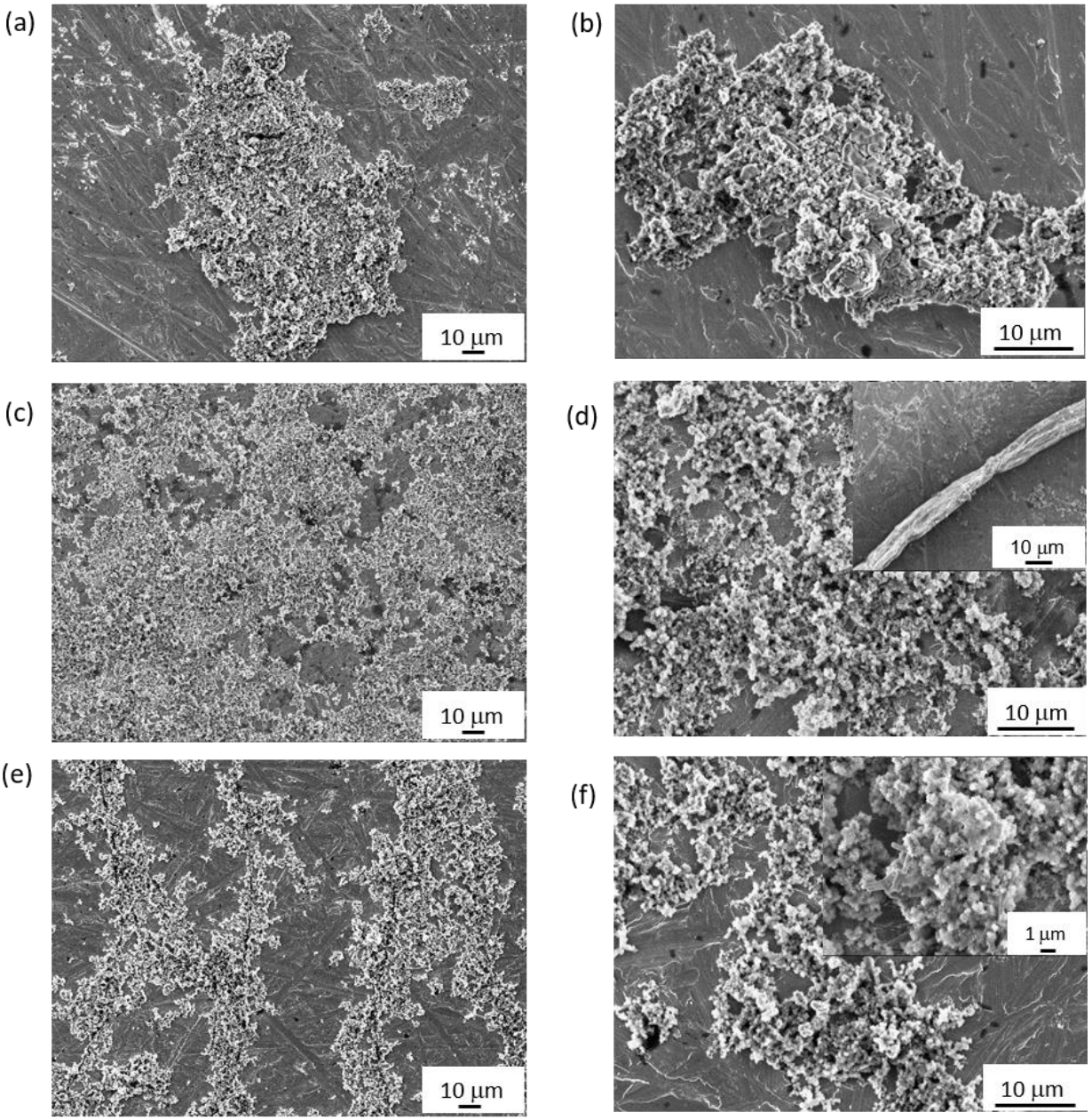


Figure 7. FE-SEM images recorded after 7 days of immersion in Fusayama artificial saliva of (a,b) bare Ti, (c,d) Ti/collagen SAM, and (e,f) Ti/collagen CV. The inset in (d) shows a detached portion of the collagen coating on the Ti/collagen SAM surface, while the inset in (f) shows a representative cluster of needle-like CaP deposits.

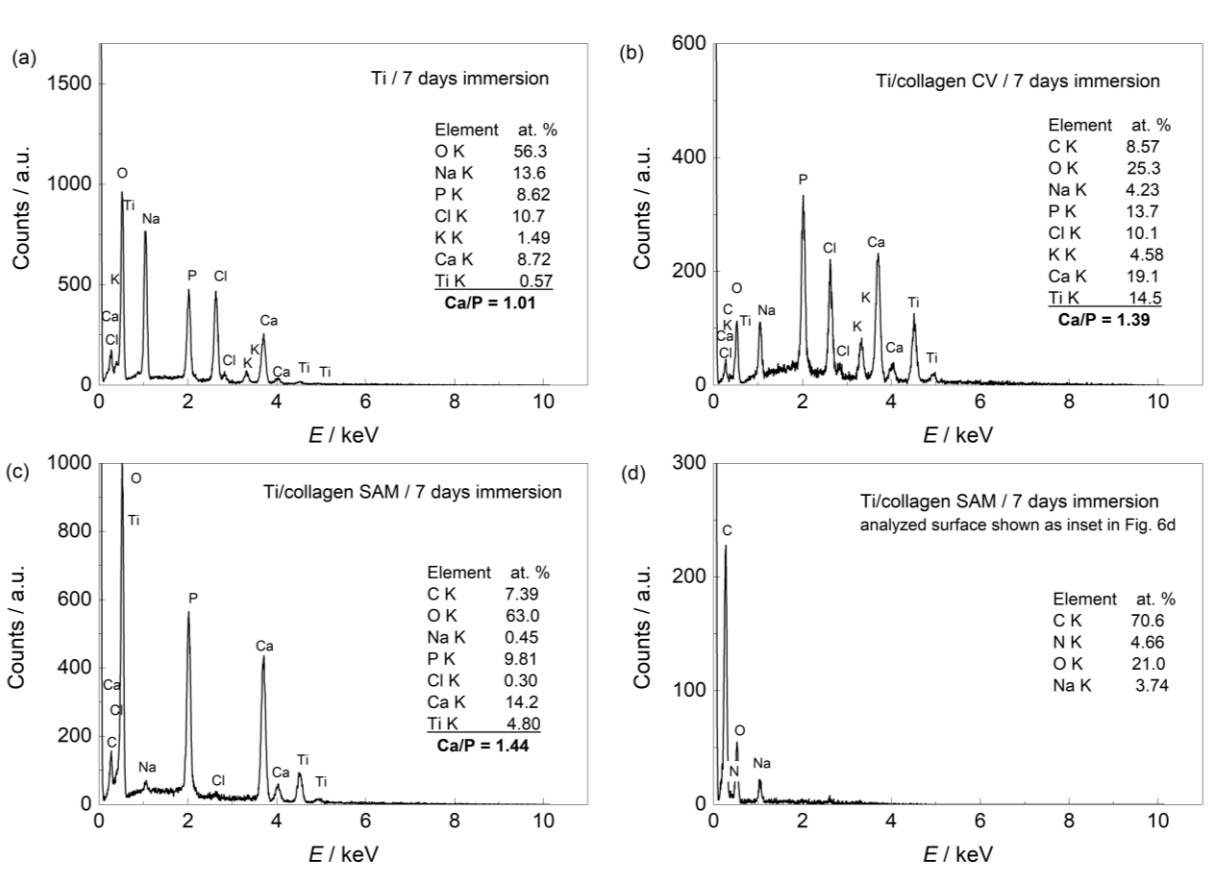


Figure 8. EDS spectra of the investigated samples after 7 days of immersion in Fusayama artificial saliva: (a) bare Ti, (b) Ti/collagen CV, and (c,d) Ti/collagen SAM surfaces. The spectrum shown in (c) represents the CaP deposits, whereas the spectrum shown in (d) represents a detached portion of the collagen coating shown as inset in Figure 7d.

XRD analysis. The phases of the CaP deposits formed on the investigated samples after 7 days of immersion in Fusayama artificial saliva were identified by XRD, and the results are shown in Figure 9.

All diffraction patterns are dominated by the reflections of the Ti substrate (ICDD PDF 00-044-1294) [45], which is expected given the low thickness of the surface deposits. Nevertheless, additional reflections associated with the newly formed CaP phases can be identified in the enlarged 20–36° 2θ region.

For bare Ti, additional reflections at approximately 28.8° and 32.1° 2θ were observed and can be assigned to β-calcium pyrophosphate (β-$Ca_2P_2O_7$; ICDD PDF 00-009-0346) [45]. In contrast, the collagen-modified surfaces exhibited reflections characteristic of hydroxyapatite (HAp; ICDD PDF 00-009-0432) [45]. For Ti/collagen SAM, reflections were observed at approximately 26.1°, 31.9°, and 32.5° 2θ, while the Ti/collagen CV surface showed reflections at approximately 25.8°, 26.2°, 32.0°, 32.4°, and 33.0° 2θ.

The XRD results identified an HAp-related phase which, together with the sub-stoichiometric Ca/P ratios obtained by EDS, is consistent with the formation of calcium-deficient (Ca-deficient) non-stoichiometric apatite relative to stoichiometric HAp (Ca/P = 1.67 [43]). The relatively broad diffraction features may further indicate low crystallinity of the deposited Ca-deficient HAp, potentially associated with structural disorder/ionic substitutions within the apatite crystal lattice [46]. Furthermore, the presence of ions such as Na, K and Cl originating from the artificial saliva was detected by EDS analysis (Figure 8).

Their presence at the surface may contribute to the observed deviation from the stoichiometric Ca/P ratio, but this is acceptable given the non-stoichiometric nature of bone-like calcium phosphates.

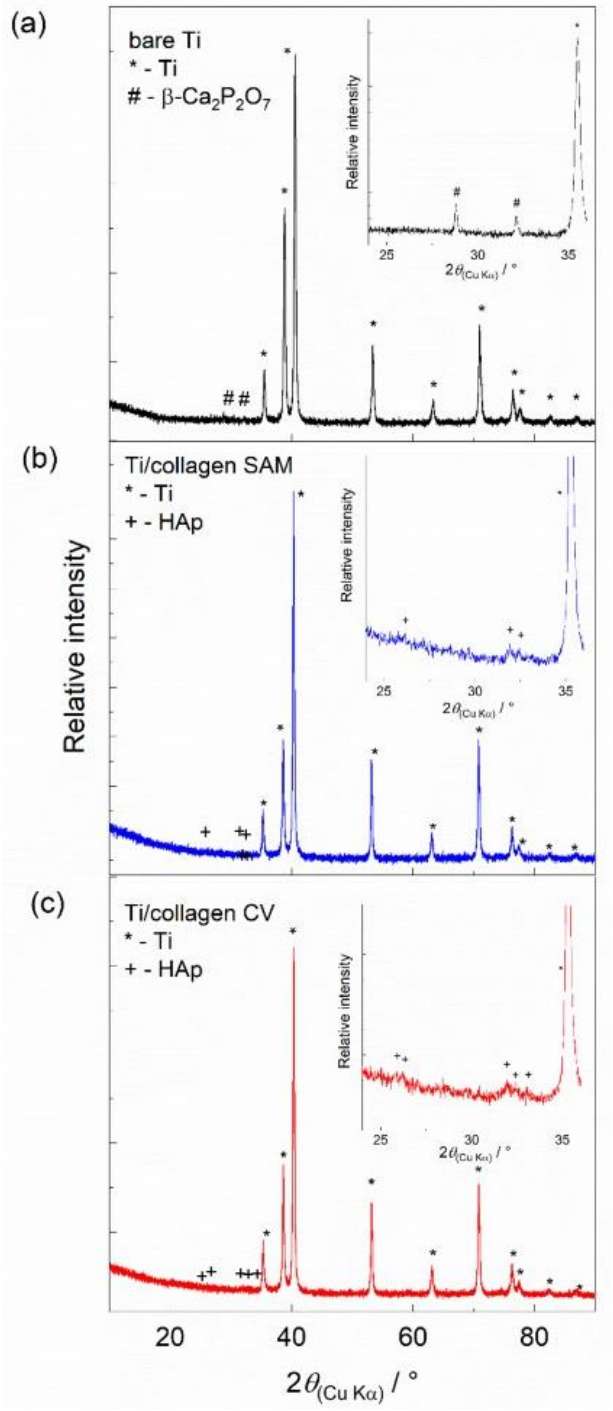


Figure 9. Diffractograms recorded in the 2θ range from 10 to 90° for (a) bare Ti, (b) Ti/collagen SAM, and (c) Ti/collagen CV. In each panel, the diffractogram of the corresponding sample recorded in the narrower 2θ range from 20 to 36° is shown as an inset. Phases are marked with symbols on the diffractograms: * – Ti (ICDD PDF 00-044-1294); + – hydroxyapatite, HAp (ICDD PDF 00-009-0432); and # – β-$Ca_2P_2O_7$ (ICDD PDF 00-009-0346).

EIS analysis. Because the processes occurring at the Ti–electrolyte interface are electrochemical in nature, it was important to investigate the electrochemical behavior of collagen-modified Ti samples during immersion in a model electrolyte of artificial saliva.

Specifically, the aim was to determine how the collagen coating changed the interface between Ti and saliva and whether its presence provided additional barrier properties to the titanium. The electrochemical behavior was investigated by EIS over a wide frequency range at the OCP at room temperature during continuous immersion in Fusayama artificial saliva for 7 days. Two immersion times were selected for detailed analysis: after 1 h and after 7 days of immersion. Before the first EIS measurement, the system was allowed to stabilize at OCP for 1 h. The EIS spectra, in the form of Bode plots, are presented in Figure 10.

Electrical equivalent circuits (EECs) were used to describe the structure of the Ti/artificial saliva and Ti/collagen/artificial saliva interfaces, and the corresponding modelling results are given in Table 1. Due to the microscopic inhomogeneities of the systems, a constant phase element (CPE) was used instead of an ideal capacitor (C) [47]. For most conditions investigated, the spectra were adequately described by an Rs(Q_1R_1) circuit, whereas the Ti/collagen CV surface after 1 h required an additional R_2C_2 relaxation, giving an Rs(Q_1[R_1(Q_2R_2)]) response [48]. R_s represents the electrolyte resistance.

The EIS responses reveal changes in the interfacial response depending on increasing immersion time for all samples investigated. For bare Ti, after just 1 h of immersion, the surface already exhibits relatively good barrier properties, as indicated by the relatively high |Z| values, which can be attributed to the presence of the spontaneously formed TiO_2-rich passive oxide layer [49]. After 7 days of immersion, the barrier properties further improve, as indicated by the increase in |Z| and broadening of the medium-frequency phase-angle response. This behavior can be associated with further development of the passive layer and the simultaneous formation of a CaP phase on the surface, as confirmed by FE-SEM, EDS, XRD and ATR-FTIR. The resulting surface film, consisting of the passive oxide layer and newly formed CaP phase, contributes to the enhanced barrier properties of the surface. In this model, R_1 represents the effective polarization resistance associated with the Ti/passive layer/Fusayama saliva interface after 1 h and with the Ti/(passive layer+ CaP)/saliva interface after 7 days, while Q_1 describes its non-ideal capacitive behavior.

In the case of the Ti/collagen SAM sample, the polarization resistance also increases substantially over the 7-day immersion period, as shown in Figure 10b. During the initial immersion period (after 1 h), the collagen coating may undergo hydration and reorganization in contact with the saliva, resulting, after 7 days, in local accumulation of collagen-rich material, as seen in the SEM results (inset in Figure 7d). With prolonged immersion (after 7 days), a new Ca-deficient HAp phase is formed on the surface, as demonstrated by XRD, ATR-FTIR, and EDS. The presence of this new phase is also reflected in the EIS response by the marked increase in |Z|, corresponding to an increase in R_1 (Table 1), and the broadening of the phase-angle response.

As for bare Ti, the EIS spectra of the Ti/collagen SAM surface were adequately described by a simple EEC. In this model, R_1 represents the effective polarization resistance associated with the Ti/collagen/Fusayama saliva interface after 1 h and the Ti/(collagen + CaP)/Fusayama saliva interface after 7 days, while Q_1 describes its non-ideal capacitive behavior. The marked increase in the resistance component of the Ti/collagen SAM surface during prolonged immersion from 0.43 MΩ cm^2 (1 h) to 1.99 MΩ cm^2 (7 days) can be associated with the formation and growth of the new Ca-deficient HAp phase. As shown by the FE-SEM and EDS results, a substantial fraction of the collagen-rich material becomes spatially separated from the CaP deposits after immersion. Thus, the contribution of the remaining collagen to the overall barrier properties appears to be less pronounced than that of the newly formed CaP phase.

The EIS results clearly show that the change in electrochemical response with immersion time in Fusayama artificial saliva is most pronounced for the Ti/collagen CV sample (Figure 10c). As shown by the SEM results, the starting surface of this sample is covered

with a porous network of collagen fibers. Therefore, the EIS data obtained after 1 h immersion were described using an EEC with two time constants. The higher-frequency time constant (Q_1R_1) can be associated with the electrochemical response of the outer fibrillar collagen framework and its interaction with the electrolyte, whereas the lower-frequency response (Q_2R_2) can be associated with electrochemical processes in the inner Ti/passive layer/collagen interfacial region. After 7 days of exposure to artificial saliva, the collagen fibers remained associated with the surface and provided a framework along which the newly formed Ca-deficient HAp phase developed, as shown SEM, XRD, EDS, and FTIR results. According to the EIS response, this formation of a new phase along/over the collagen fibers was reflected in a pronounced broadening of the phase-angle response and a marked increase in the barrier properties of this sample. The EIS response is then adequately described by an EEC with one time constant, representing the effective polarization resistance at the Ti/(collagen+CaP)/saliva interface and its non-ideal capacitive behavior. The total resistance ($R_1 + R_2$) of the interfacial system increased from 0.54 MΩ cm² after 1 h to 6.20 MΩ cm² after 7 days of immersion, corresponding to an increase of more than one order of magnitude (Table 1). This pronounced increase in barrier resistance can be related to the combined contribution of the retained collagen fibers and the newly formed Ca-deficient HAp phase. Thus, unlike the SAM coating, where the increase in resistance appears to be predominantly associated with Ca-deficient HAp formation, the electrochemically formed coating retained an organic–inorganic interfacial architecture in which both collagen and the Ca-deficient phase contribute to the enhanced barrier properties.

Overall, the results of the comprehensive multi-technique characterization clearly demonstrate that the formation method significantly influences the architecture of the collagen coating, which in turn determines its interfacial behavior during immersion in artificial saliva. The EIS results demonstrate that the investigated surfaces follow different interfacial evolution pathways during immersion. Bare Ti exhibits a relatively stable passive response, with an increase in barrier resistance associated with the development of the CaP surface layer. The Ti/collagen SAM surface also shows an increase in resistance during prolonged immersion, which appears to be mainly associated with the development of the CaP surface layer. In contrast, the Ti/collagen CV surface exhibits the highest barrier resistance after 7 days, consistent with the retention of the collagen fibers and their close association with the newly formed CaP phase. The resulting organic–inorganic surface architecture is associated with enhanced electrochemical barrier properties compared with unmodified Ti.

Table 1. EIS fitting parameters obtained for bare Ti, Ti/collagen SAM and Ti/collagen CV after 1 h and 7 days of immersion in Fusayama artificial saliva.

Samples	R_s / Ω cm²	$Q_1 \cdot 10^6$ / Ω^{-1} cm^{-2} s^{n1}	n_1	R_1 / MΩ cm²	$Q_2 \cdot 10^6$ / Ω^{-1} cm^{-2} s^{n2}	n_2	R_2 / MΩ cm²	$\chi^2 * 10^{-3}$
bare Ti								
1h	197	44.2	0.888	0.35				2.0
7 days	196	36.1	0.908	1.98	/			2.8
Ti/collagen SAM								
1h	205	40.4	0.912	0.43	/	/	/	1.5
7 days	196	36.1	0.908	1.99	/	/	/	2.8
Ti/collagen CV								
1h	113	36.4	0.897	0.33	136	0.909	0.21	1.1
7 days	260	35.7	0.924	6.20	/	/	/	1.7

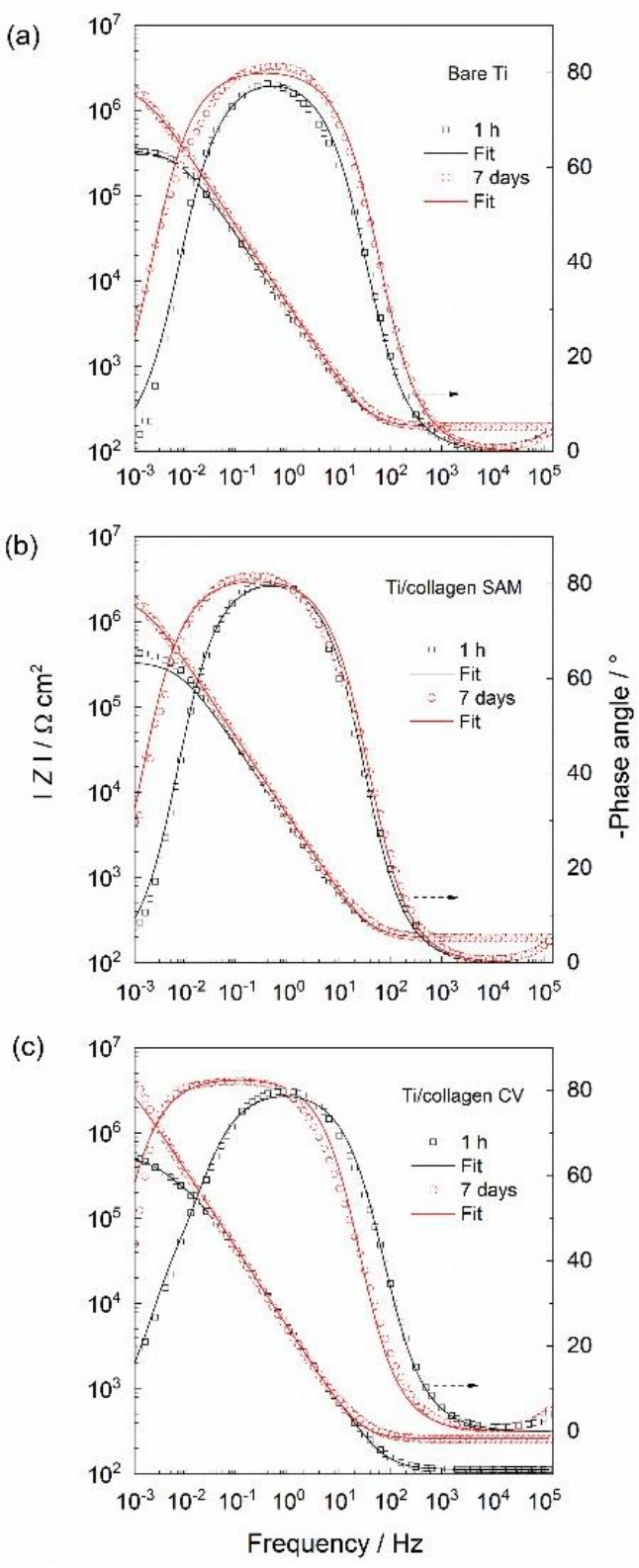


Figure 10. Bode plots showing the impedance modulus and phase angle of (a) bare Ti, (b) Ti/collagen SAM, and (c) Ti/collagen CV during immersion in Fusayama artificial saliva. Experimental data (symbols) recorded after 1 h and 7 days of immersion are shown together with the corresponding fits (lines).

3.6. Time-dependent Ti release and cell viability

Titanium concentrations remained low throughout the 90-day incubation period in cell media (Figures 11a,b), with no pronounced time-dependent increase in Ti release for most samples. Comparably low levels of titanium release have previously been reported for titanium dental materials under simulated physiological conditions [50]. A higher Ti concentration of 12.96 μg L^{-1} was detected only in one aliquot of FBS-supplemented medium after 90 days. However, this value was substantially lower than the 20 ppm Ti concentration reported in another in vitro model to significantly reduce cell viability after 24 h exposure [51]. To assess possible biological effects, HGF-1 and MG-63 cells were exposed for 24 h to the corresponding conditioned media (Figures 11c,d). No reduction in cell viability was observed for either cell line, irrespective of incubation time, serum supplementation, or collagen modification. This is consistent with previous reports showing that adverse cellular effects of titanium are mainly observed at substantially higher Ti concentrations than those detected here [51]. Moreover, collagen modification did not affect cytocompatibility, in agreement with previous studies on collagen-coated titanium surfaces [52].

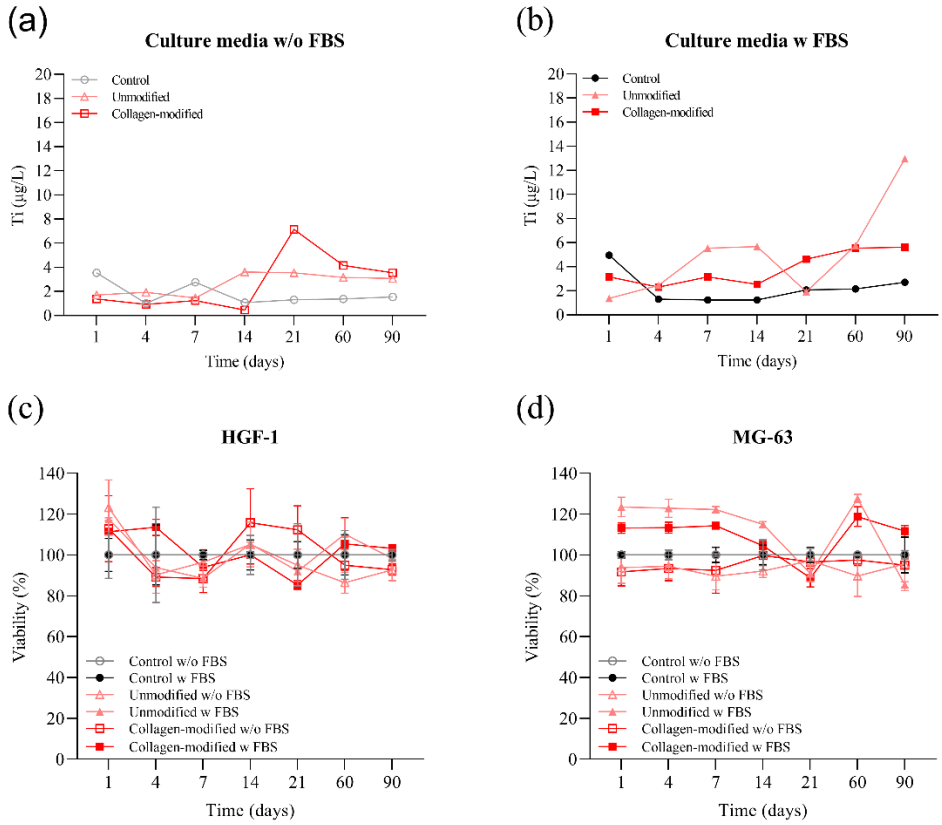


Figure 11. Ti release concentration over 90 days in cell culture medium (a) without and (b) supplemented with fetal bovine serum (FBS), and cell viability of (c) HGF-1 and (d) MG-63 cells after 24 h exposure to conditioned media collected during the 90-day titanium release study. Open symbols represent serum-free conditions, whereas filled symbols represent FBS-supplemented conditions. Circles indicate the control, triangles represent unmodified Ti, and squares represent collagen-modified Ti.

4. Conclusions

This work investigated the influence of collagen coating preparation methods on coating´s architecture and the subsequent behavior of modified Ti surfaces during immersion in Fusayama artificial saliva. Ti release and indirect in vitro cytocompatibility were additionally evaluated to provide an initial assessment of the biological response. Two approaches were used to form the collagen coatings: chemical self-assembly and electrochemical formation by cyclic voltammetry. Based on the results of the comprehensive characterization, the following conclusions can be drawn:

- Collagen coatings were successfully formed on Ti by both preparation methods, as confirmed primarily by ATR-FTIR and supported by FE-SEM and EDS analyses.
- FE-SEM results clearly demonstrated that the coating formation method strongly affected coating morphology. Chemical self-assembly yielded a relatively continuous collagen layer with locally accumulated island-like structures, whereas cyclic voltammetry produced a distinctly different morphology dominated by overlapping collagen fibers forming a network-like structure.
- DFT calculations revealed that electrochemical oxidation of the modelled anionic Gly–Pro–Hyp tripeptide adsorbed on TiO_2 induces structural changes, including substantial elongation of the C–C bond connecting the hydroxyproline ring to its carboxylate carbon. These changes may facilitate intermolecular C–N coupling and subsequent peptide-like chain growth. However, because the calculated oxidation potential (+0.458 V vs Ag/AgCl/3 M KCl) lies above the upper vertex potential (+0.1 V) applied during CV coating formation, the calculated oxidation pathway cannot be directly assigned as the mechanism responsible for the experimentally observed fibrillar coating morphology.
- The different coating morphologies were associated with distinct interfacial evolution and mineralization patterns during 7-day exposure to Fusayama artificial saliva. Combined XRD, ATR-FTIR, and EDS results supported the formation of a calcium-deficient, non-stoichiometric apatite phase on both modified surfaces, with Ca/P atomic ratios of 1.44 for Ti/collagen SAM and 1.39 for Ti/collagen CV. Despite their similar Ca/P ratios, the spatial organization of the deposits differed: Ca-deficient apatite deposits appeared to develop preferentially along and around the retained collagen fibers in the CV coating, whereas the SAM coating underwent reorganization, with partially detached collagen-rich regions observed after immersion.
- The influence of the coating architectures was most evident in the electrochemical barrier properties determined by EIS measurements in artificial saliva. After 7 days of immersion, the Ti/collagen CV surface showed a pronounced increase in barrier resistance, reaching 6.20 MΩ cm², compared with 1.98 and 1.99 MΩ cm² for bare Ti and Ti/collagen SAM, respectively. The enhanced barrier resistance of the Ti/collagen CV sample was associated with retention of the collagen fibrillar framework and its close spatial association with the newly formed Ca-deficient apatite phase, as indicated by the complementary characterization results.
- The tested Ti and Ti/collagen samples exhibited low Ti release during prolonged exposure to cell culture media, while the corresponding conditioned media showed no significant adverse effects on human gingival fibroblasts

(HGF-1) or osteoblast-like (MG-63) cells in the studied experimental conditions, supporting favorable indirect in vitro cytocompatibility under the investigated conditions.

Author Contributions: "Conceptualization, Ž.P. and I.D.; methodology, Ž.P. and I.D.; validation, M.I. Ž.P., and A.Z.; formal analysis, J.K., I.D., and Ž.P.; investigation, M.H., A.Z., and M.I.; resources, I.D., M.K., and Ž.P.; data curation, I.D. and Ž.P.; writing—original draft preparation, Ž.P., I.D. A.Z.; writing—review and editing, Ž.P., I.D., M.K.; visualization, Ž.P., I.D., A.Z.; supervision, Ž.P. All authors have read and agreed to the published version of the manuscript

Funding: The research was partially funded by NextGenerationEU (GD1-26; 01/753/2-2026) and NextGenerationEU (BioMolTox, Class: 643-02/23-01/00016, Reg. no. 533-03-23-0006).

Data Availability Statement: The data presented in this study are available on request from the corresponding author.

Acknowledgments: The authors thank the Zagreb University Computing Centre (SRCE) for generously providing computational resources on the SUPEK supercomputer. The authors also thank Đurđica Brlek for her technical assistance with the XRD measurements and the staff of the Radiation Chemistry and Dosimetry Laboratory of the Ruđer Bošković Institute for the sterilization of the samples. Part of this study was performed using the facilities and equipment funded within the ERDF project KK.01.1.1.02.0007 "Research and Education Centre of Environmental Health and Radiation Protection–Reconstruction and Expansion of the Institute for Medical Research and Occupational Health".

Generative AI statement: During the preparation of this manuscript, the authors used OpenAI ChatGPT (GPT-5.6 Sol) for the visual composition and design of the Graphical Abstract. The authors reviewed and edited the output and take full responsibility for the content of this publication.

Conflicts of Interest: The authors declare no conflicts of interest.

References

1. Boyan, B.D.; Batzer, R.; Kieswetter, K.; Liu, Y.; Cochran, D.L.; Szmuckler-Moncler, S.; Dean, D.D.; Schwartz, Z. Titanium surface roughness alters responsiveness of MG63 osteoblast-like cells to 1α,25-$(OH)_2D_3$. *J. Biomed. Mater. Res.* **1998**, *39*, 77–85. https://doi.org/10.1002/(SICI)1097-4636(199801)39:1<77::AID-JBM10>3.0.CO;2-L
2. Buser, D.; Schenk, R.K.; Steinemann, S.; Fiorellini, J.P.; Fox, C.H.; Stich, H. Influence of surface characteristics on bone integration of titanium implants. A histomorphometric study in miniature pigs. *J. Biomed. Mater. Res.* **1991**, *25*, 889–902. https://doi.org/10.1002/jbm.820250708
3. Jadhav, L.; Madiwal, V.; Rajwade, J.M. The dental implant surface: A review of the past, present and future. *J. Mater. Sci. Mater. Med.* **2026**, *37*, 21. https://doi.org/10.1007/s10856-025-06997-x
4. Banerjee, U.; Dhawan, P.; Jain, N.; Naidu, S. Enhancing biological response and bone-implant contact through surface treatment of dental implants: Exploring contemporary techniques. *J. Adv. Med. Med. Res.* **2025**, *37*, 195–211. https://doi.org/10.9734/jammr/2025/v37i115978
5. Schupbach, P.; Glauser, R.; Bauer, S. Al_2O_3 particles on titanium dental implant systems following sandblasting and acid-etching process. *Int. J. Biomater.* **2019**, *2019*, 6318429. https://doi.org/10.1155/2019/6318429
6. He, W.; Yin, X.; Xie, L.; Liu, Z.; Li, J.; Zou, S.; Chen, J. Enhancing osseointegration of titanium implants through large-grit sandblasting combined with micro-arc oxidation surface modification. *J. Mater. Sci. Mater. Med.* **2019**, *30*, 73. https://doi.org/10.1007/s10856-019-6276-0
7. Choi, A.H.; Ben-Nissan, B.; Matinlinna, J.P.; Conway, R.C. Current perspectives: Calcium phosphate nanocoatings and nanocomposite coatings in dentistry. *J. Dent. Res.* **2013**, *92*, 853–859. https://doi.org/10.1177/0022034513497754
8. Kämmerer, P.W.; Pabst, A.M.; Dau, M.; Staedt, H.; Al-Nawas, B.; Heller, M. Immobilization of BMP-2, BMP-7 and alendronic acid on titanium surfaces: Adhesion, proliferation and differentiation of bone marrow-derived stem cells. *J. Biomed. Mater. Res. A* **2020**, *108*, 212–220. https://doi.org/10.1002/jbm.a.36805

9. Liu, C.-F.; Chang, K.-C.; Sun, Y.-S.; Nguyen, D.T.; Huang, H.-H. Combining sandblasting, alkaline etching, and collagen immobilization to promote cell growth on biomedical titanium implants. *Polymers* **2021**, *13*, 2550. https://doi.org/10.3390/polym13152550
10. Al Shayeb, M.; Elfadil, S.; Abutayyem, H.; Shqaidef, A.; Marrapodi, M.M.; Cicciù, M.; Minervini, G. Bioactive surface modifications on dental implants: A systematic review and meta-analysis of osseointegration and longevity. *Clin. Oral Investig.* **2024**, *28*, 592. https://doi.org/10.1007/s00784-024-05958-y
11. Sverzut, A.T.; Crippa, G.E.; Morra, M.; de Oliveira, P.T.; Beloti, M.M.; Rosa, A.L. Effects of type I collagen coating on titanium osseointegration: Histomorphometric, cellular and molecular analyses. *Biomed. Mater.* **2012**, *7*, 035007. https://doi.org/10.1088/1748-6041/7/3/035007
12. Scarano, A.; Lorusso, F.; Orsini, T.; Morra, M.; Iviglia, G.; Valbonetti, L. Biomimetic surfaces coated with covalently immobilized collagen type I: An X-ray photoelectron spectroscopy, atomic force microscopy, micro-CT and histomorphometrical study in rabbits. *Int. J. Mol. Sci.* **2019**, *20*, 724. https://doi.org/10.3390/ijms20030724
13. Morra, M.; Cassinelli, C.; Meda, L.; Fini, M.; Giavaresi, G.; Giardino, R. Surface analysis and effects on interfacial bone microhardness of collagen-coated titanium implants: A rabbit model. *Int. J. Oral Maxillofac. Implants* **2005**, *20*, 23–30. PMID: 15747670.
14. Marín-Pareja, N.; Salvagni, E.; Guillem-Marti, J.; Aparicio, C.; Ginebra, M.-P. Collagen-functionalised titanium surfaces for biological sealing of dental implants: Effect of immobilisation process on fibroblasts response. *Colloids Surf. B Biointerfaces* **2014**, *122*, 601–610. https://doi.org/10.1016/j.colsurfb.2014.07.038
15. Gregurec, D.; Wang, G.; Pires, R.H.; Kosutic, M.; Lüdtke, T.; Delcea, M.; Moya, S.E. Bioinspired titanium coatings: Self-assembly of collagen–alginate films for enhanced osseointegration. *J. Mater. Chem. B* **2016**, *4*, 1978–1986. https://doi.org/10.1039/C6TB00204H
16. Petrović, Ž.; Šarić, A.; Despotović, I.; Katić, J.; Peter, R.; Petravić, M.; Ivanda, M.; Petković, M. Surface functionalisation of dental implants with a composite coating of alendronate and hydrolysed collagen: DFT and EIS studies. *Materials* **2022**, *15*, 5127. https://doi.org/10.3390/ma15155127
17. Wang, M.; Jiang, M.; Wang, Q.; Sun, Y.; Nie, Z.; Palin, W.M.; Zhang, Z. An in vitro bioinspired approach to enhance the bioactivity of titanium implants via electrophoretic deposition and biomimetic mineralization of type I collagen. *Biomater. Adv.* **2025**, *167*, 214110. https://doi.org/10.1016/j.bioadv.2024.214110
18. Kamata, H.; Suzuki, S.; Tanaka, Y.; Tsutsumi, Y.; Doi, H.; Nomura, N.; Hanawa, T.; Moriyama, K. Effects of pH, potential, and deposition time on the durability of collagen electrodeposited to titanium. *Mater. Trans.* **2011**, *52*, 81–89. https://doi.org/10.2320/matertrans.M2010311
19. Petrović, Ž.; Despotović, I.; Katić, J. The DFT structure–property relationship of titanium functionalized with electrochemically deposited collagen fibrils. *J. Coat. Technol. Res.* **2026**, *23*, 1461–1478. https://doi.org/10.1007/s11998-025-01192-7
20. Mellado-Valero, A.; Igual Muñoz, A.; Guiñón Pina, V.; Sola-Ruiz, M.F. Electrochemical behaviour and galvanic effects of titanium implants coupled to metallic suprastructures in artificial saliva. *Materials* **2018**, *11*, 171. https://doi.org/10.3390/ma11010171
21. **JEOL Windowless EDS Periodic Table.** Available online: https://www.jeolusa.com/Portals/2/brochures/JEOL%20Windowless%20EDS%20Periodic%20Table.jpg?ver=H48zbGcPTUTqtWCa82HCiw%3d%3d (accessed on 15 September 2025).
22. Qu, Z.; Kroes, G.-J. Theoretical study of stable, defect-free $(TiO_2)_n$ nanoparticles with $n = 10–16$. *J. Phys. Chem. C* **2007**, *111*, 16808–16817. https://doi.org/10.1021/jp073988t
23. Hohenberg, P.; Kohn, W. Inhomogeneous electron gas. *Phys. Rev.* **1964**, *136*, B864–B871. https://doi.org/10.1103/PhysRev.136.B864
24. Kohn, W.; Sham, L.J. Self-consistent equations including exchange and correlation effects. *Phys. Rev.* **1965**, *140*, A1133–A1138. https://doi.org/10.1103/PhysRev.140.A1133
25. Zhao, Y.; Truhlar, D.G. The M06 suite of density functionals for main group thermochemistry, thermochemical kinetics, noncovalent interactions, excited states, and transition elements: Two new functionals and systematic testing of four M06-class functionals and 12 other functionals. *Theor. Chem. Acc.* **2008**, *120*, 215–241. https://doi.org/10.1007/s00214-007-0310-x
26. Zhao, Y.; Truhlar, D.G. Density functionals with broad applicability in chemistry. *Acc. Chem. Res.* **2008**, *41*, 157–167. https://doi.org/10.1021/ar700111a
27. Zhao, Y.; Truhlar, D.G. Density functional theory for reaction energies: Test of meta and hybrid meta functionals, range-separated functionals, and other high-performance functionals. *J. Chem. Theory Comput.* **2011**, *7*, 669–676. https://doi.org/10.1021/ct1006604
28. Wadt, W.R.; Hay, P.J. *Ab initio* effective core potentials for molecular calculations. Potentials for main group elements Na to Bi. *J. Chem. Phys.* **1985**, *82*, 284–298. https://doi.org/10.1063/1.448800

29. Marenich, A.V.; Cramer, C.J.; Truhlar, D.G. Universal solvation model based on solute electron density and on a continuum model of the solvent defined by the bulk dielectric constant and atomic surface tensions. *J. Phys. Chem. B* **2009**, *113*, 6378–6396. https://doi.org/10.1021/jp810292n
30. Frisch, M.J.; Trucks, G.W.; Schlegel, H.B.; Scuseria, G.E.; Robb, M.A.; Cheeseman, J.R.; Scalmani, G.; Barone, V.; Petersson, G.A.; Nakatsuji, H.; et al. *Gaussian 16*, Revision C.01; Gaussian, Inc.: Wallingford, CT, USA, 2019.
31. Bader, R.F.W. *Atoms in Molecules: A Quantum Theory*; Oxford University Press: Oxford, UK, 1990. https://doi.org/10.1093/oso/9780198551683.001.0001
32. Keith, T.A. *AIMAll*, Version 17.01.25; TK Gristmill Software: Overland Park, KS, USA, 2017. Available online: https://aim.tkgristmill.com/ (accessed on 20 October 2026).
33. Gritzner, G.; Kuta, J. Recommendations on reporting electrode potentials in nonaqueous solvents (Provisional). *Pure Appl. Chem.* **1982**, *54*, 1527–1532. https://doi.org/10.1351/pac198254081527
34. Trasatti, S. The absolute electrode potential: An explanatory note (Recommendations 1986). *Pure Appl. Chem.* **1986**, *58*, 955–966. https://doi.org/10.1351/pac198658070955
35. Boniolo, M.; Hossain, M.K.; Chernev, P.; Suremann, N.F.; Heizmann, P.A.; Lyvik, A.S.L.; Beyer, P.; Haumann, M.; Huang, P.; Salhi, N.; Cheah, M.H.; Shylin, S.I.; Lundberg, M.; Thapper, A.; Messinger, J. Water oxidation by pentapyridyl base metal complexes? A case study. *Inorg. Chem.* **2022**, *61*, 9104–9118. https://doi.org/10.1021/acs.inorgchem.2c00631
36. de Almeida, T.C.S.; Valverde, T.M.; Martins, T.M.M.; Oliveira, F.P.; Cunha, P.S.; Tavares, M.A.B.; Rodrigues, E.M.; Albergaria, J.D.S.; Vieira, G.M.; Gomes, D.A.; Gastelois, P.L.; de Souza, R.L.; de Góes, A.M.; Kitten, G.T.; Martins, M.D. Enhanced osteogenic response by collagen type I coating on surface-modified titanium bone implants. *Mater. Today Commun.* **2024**, *39*, 108535. https://doi.org/10.1016/j.mtcomm.2024.108535
37. Zandona, A.; Zorbaz, T.; Miš, K.; Pirkmajer, S.; Katalinić, M. Cytotoxicity-related effects of imidazolium and chlorinated bispyridinium oximes in SH-SY5Y cells. *Arh. Hig. Rada Toksikol.* **2022**, *73*, 277–284. https://doi.org/10.2478/aiht-2022-73-3688
38. de Campos Vidal, B.; Mello, M.L.S. Collagen type I amide I band infrared spectroscopy. *Micron* **2011**, *42*, 283–289. https://doi.org/10.1016/j.micron.2010.09.010
39. Günzler, H.; Gremlich, H.-U. *IR-Spektroskopie: Eine Einführung*, 4th ed.; Wiley-VCH: Weinheim, Germany, 2003. https://doi.org/10.1002/9783527662852
40. Petrović, Ž.; Metikoš-Huković, M.; Omanovic, S.; Leskovac, M. Structural and protecting properties of functional organic coatings on copper. *ECS Trans.* **2010**, *28*, 51–63. https://doi.org/10.1149/1.3502444
41. Bae, E.-B.; Yoo, J.-H.; Jeong, S.-I.; Kim, M.-S.; Lim, Y.-M.; Ahn, J.-J.; Lee, J.-J.; Lee, S.-H.; Kim, H.-J.; Huh, J.-B. Effect of titanium implants coated with radiation-crosslinked collagen on stability and osseointegration in rat tibia. *Materials* **2018**, *11*, 2520. https://doi.org/10.3390/ma11122520
42. Cho, W.-T.; Kim, S.-Y.; Jung, S.-I.; Kang, S.-S.; Kim, S.-E.; Hwang, S.-H.; Jeong, C.-M.; Huh, J.-B. Effects of gamma radiation-induced crosslinking of collagen type I coated dental titanium implants on osseointegration and bone regeneration. *Materials* **2021**, *14*, 3268. https://doi.org/10.3390/ma14123268
43. Berzina-Cimdina, L.; Borodajenko, N. Research of calcium phosphates using Fourier transform infrared spectroscopy. In *Infrared Spectroscopy—Materials Science, Engineering and Technology*; Theophanides, T., Ed.; IntechOpen: Rijeka, Croatia, 2012. https://doi.org/10.5772/36942
44. Diez-Escudero, A.; Espanol, M.; Ginebra, M.-P. High-aspect-ratio nanostructured hydroxyapatite: Towards new functionalities for a classical material. *Chem. Sci.* **2024**, *15*, 55–76. https://doi.org/10.1039/D3SC05344
45. International Centre for Diffraction Data (ICDD). *Powder Diffraction File Search*. Available online: https://www.icdd.com/pdf-search/ (accessed on 10 April 2026).
46. Lin, K.; Zhou, Y.; Zhou, Y.; Qu, H.; Chen, F.; Zhu, Y.; Chang, J. Biomimetic hydroxyapatite porous microspheres with co-substituted essential trace elements: Surfactant-free hydrothermal synthesis, enhanced degradation and drug release. *J. Mater. Chem.* **2011**, *21*, 16558–16565. https://doi.org/10.1039/C1JM12514A
47. Orazem, M.E.; Tribollet, B. *Electrochemical Impedance Spectroscopy*; Wiley: Hoboken, NJ, USA, 2008; pp. 233–265. https://doi.org/10.1002/9780470381588
48. Harrington, D.A.; van den Driessche, P. Mechanism and equivalent circuits in electrochemical impedance spectroscopy. *Electrochim. Acta* **2011**, *56*, 8005–8013. https://doi.org/10.1016/j.electacta.2011.01.067
49. Eliaz, N. Corrosion of metallic biomaterials: A review. *Materials* **2019**, *12*, 407. https://doi.org/10.3390/ma12030407

851 50. Silva Salas, D.J.; Ocariz De Colina, M.; Monteverde-La Roche, C.; Terrero-Reyes, D.; Argüello-Lacayo, L.; Galvez-Armas, K.;
852 Rodriguez, L.S. Tribochemical degradation at the implant-abutment interface and its implications for marginal bone loss and
853 peri-implant mucositis: A narrative review. *Cureus* **2026**, *18*, e115969. https://doi.org/10.7759/cureus.115969
854 51. Mine, Y.; Makihira, S.; Nikawa, H.; Murata, H.; Hosokawa, R.; Hiyama, A.; Mimura, S. Impact of titanium ions on osteoblast-,
855 osteoclast- and gingival epithelial-like cells. *J. Prosthodont. Res.* **2010**, *54*, 1–6. https://doi.org/10.1016/j.jpor.2009.07.003
856 52. Rammelt, S.; Schulze, E.; Bernhardt, R.; Hanisch, U.; Scharnweber, D.; Worch, H.; Zwipp, H.; Biewener, A. Coating of titanium
857 implants with type-I collagen. *J. Orthop. Res.* **2004**, *22*, 1025–1034. https://doi.org/10.1016/j.orthres.2004.02.011

858 **Disclaimer/Publisher's Note:** The statements, opinions and data contained in all publications are solely those of the individual au-
859 thor(s) and contributor(s) and not of MDPI and/or the editor(s). MDPI and/or the editor(s) disclaim responsibility for any injury to
860 people or property resulting from any ideas, methods, instructions or products referred to in the content.